NASA/TM-2018-219976

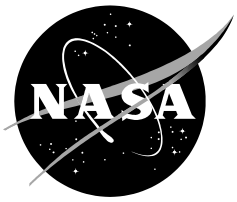

Intermittency and Cessation of Vortex Shedding in the Wake of a Thin Flat Plate with a Circular Trailing Edge

Man Mohan Rai
Ames Research Center
Moffett Field, CA-94035

August 2018

NASA STI Program ... in Profile

Since its founding, NASA has been dedicated to the advancement of aeronautics and space science. The NASA scientific and technical information (STI) program plays a key part in helping NASA maintain this important role.

The NASA STI program operates under the auspices of the Agency Chief Information Officer. It collects, organizes, provides for archiving, and disseminates NASA's STI. The NASA STI program provides access to the NTRS Registered and its public interface, the NASA Technical Reports Server, thus providing one of the largest collections of aeronautical and space science STI in the world. Results are published in both non-NASA channels and by NASA in the NASA STI Report Series, which includes the following report types:

- TECHNICAL PUBLICATION. Reports of completed research or a major significant phase of research that present the results of NASA Programs and include extensive data or theoretical analysis. Includes compilations of significant scientific and technical data and information deemed to be of continuing reference value. NASA counterpart of peer-reviewed formal professional papers but has less stringent limitations on manuscript length and extent of graphic presentations.

- TECHNICAL MEMORANDUM. Scientific and technical findings that are preliminary or of specialized interest, e.g., quick release reports, working papers, and bibliographies that contain minimal annotation. Does not contain extensive analysis.

- CONTRACTOR REPORT. Scientific and technical findings by NASA-sponsored contractors and grantees.

- CONFERENCE PUBLICATION. Collected papers from scientific and technical conferences, symposia, seminars, or other meetings sponsored or co-sponsored by NASA.

- SPECIAL PUBLICATION. Scientific, technical, or historical information from NASA programs, projects, and missions, often concerned with subjects having substantial public interest.

- TECHNICAL TRANSLATION. English-language translations of foreign scientific and technical material pertinent to NASA's mission.

Specialized services also include organizing and publishing research results, distributing specialized research announcements and feeds, providing information desk and personal search support, and enabling data exchange services.

For more information about the NASA STI program, see the following:

- Access the NASA STI program home page at http://www.sti.nasa.gov

- E-mail your question to help@sti.nasa.gov

- Phone the NASA STI Information Desk at 757-864-9658

- Write to:
  NASA STI Information Desk
  Mail Stop 148
  NASA Langley Research Center
  Hampton, VA 23681-2199

NASA/TM-2018-219976

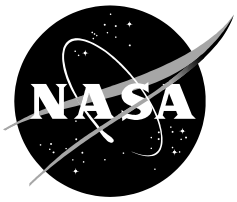

Intermittency and Cessation of Vortex Shedding in the Wake of a Thin Flat Plate with a Circular Trailing Edge

Man Mohan Rai
Ames Research Center
Moffett Field, California

National Aeronautics and
Space Administration

Ames Research Center
Moffett Field, California 94035-1000

August 2018

INTERMITTENCY AND CESSATION OF VORTEX SHEDDING IN THE WAKE OF A THIN FLAT PLATE WITH A CIRCULAR TRAILING EDGE

Man Mohan Rai*
NASA Ames Research Center, Moffett Field, CA-94035, USA

ABSTRACT

The near and very near wake of thin flat plates with both sharp and circular trailing edges (TEs) are investigated with direct numerical simulations (DNSs). The TE is circular in two of the cases (IN & NS) and sharp in one of them (ST). The separating boundary layers are turbulent in all cases. The objectives of this study are twofold. The first is to explore the effect of significantly reducing Re_D (Reynolds number based on circular TE diameter, D) on the flow in the TE region, and the shedding process (Cases IN and NS). The second is to better understand the reasons underlying the findings of an earlier experimental wake investigation (sharp TE) where (1) the center-line values in normal intensity, and the peak in shear stress profiles in the cross-stream direction, were found to first increase in the streamwise direction (x), from that obtained at the TE, before diminishing further downstream, and (2) a broadband peak was observed in centerline cross-stream velocity (*v*) spectra (indicating quasi-periodicity, possibly due to vortices or wave-like motions). Case ST from the present study showed a near wake instability resulting in spanwise vortices (with a streamwise component). The instability is intermittent and contributes to both the broadband peak in the *v* spectrum and the initial increases in normal intensity and shear stress (as in the experiment). Case NS, with the lower value of Re_D is an "essentially" non-shedding case where the flow in the TE region continually changes direction (upward/downward) because of turbulence. Case IN, with twice the value of Re_D as Case NS, also exhibits a swaying motion in the TE region. In addition, vortex shedding is initiated during periods when the flow direction changes rapidly. Shedding in this case is intermittent. It results in a peak in the *v* spectrum obtained at the centerline (x/D = 1.0).

1. INTRODUCTION

An extensive investigation of the wake of the thick flat plate with a circular trailing edge and turbulent separating boundary layers, was initiated by Rai (2013, 2014 & 2015). This was accomplished with the aid of direct numerical simulations (DNSs). The boundary layers as well as the wake were computed via DNS in these investigations. The separating boundary layers are fully turbulent well upstream of the trailing edge (TE) and are statistically identical. The wake is symmetric in the mean and vortex shedding is vigorous in all the cases investigated (Cases A - D). Unlike the case of the cylinder, the Reynolds number based on momentum thickness of the boundary layer just upstream of the TE (Re_θ) and the Reynolds number defined using the thickness of the flat plate **or** the diameter of its TE (Re_D), are independent parameters. Collectively, the articles by Rai (2013, 2014 & 2015) address several aspects of the flat plate wake such as the instability of the detached shear layers (DSLs), entrainment, the distribution of phase-averaged turbulence intensities and shear stress and associated production terms.

The objective of the more recent investigations by Rai (2017, 2018) is to understand the changes in the characteristics of the wake of a flat plate with turbulent separating boundary layers (in particular changes in vortex shedding), as the plate becomes thin in *relation* to the boundary layer thickness (increasing θ/D). The TE of the plate *remained circular* in the cases investigated in these two articles. Changes obtained with increasing θ/D, in the coherence of the shed vortices (spanwise direction, z), in the roll-up of the DSLs and time-averaged velocity statistics are discussed. The continuity of the shedding

* Senior Researcher, Computational Sciences, Exploration Technology Directorate.

process is demonstrated and the appearance of significant variation in shedding intensity and frequency is noted in these articles. Important contributors to the substantial changes in the observed flow features as θ/D is increased are identified.

The five cases investigated in Rai (2017, 2018) are labeled Cases A, D, E, F & G. Case A is the reference case (thick plate). Values of Re_D and the ratio $\psi = (\theta/D)/(\theta/D)_{Case\ A}$ for these five cases are provided in Table 1. The ratio ψ is essential in comparing the value of (θ/D) for any given case to that of the reference case (Case A); it varies substantially over the cases considered (by a factor of 51.6). Table 1 also provides the value of ψ for the two new cases with a circular TE, computed during the present investigation, Cases IN & NS. The Reynolds number based on plate length L is the same in all these cases, $Re_L = 1.25 \times 10^6$. The plate length is the same in Case ST as well, but the TE is sharp; the thickness of the plate prior to the tapered end is the same as in Case F and the TE wedge angle is 0.4^o.

	Re_D	ψ
Case A	10,000	1.0
Case D	5000	2.3
Case E	2500	4.9
Case F	625	20.4
Case G	250	51.6
Case IN	100	129.0
Case NS	50	258.0

Table 1. The parameters Re_D and ψ for Cases A, D, E, F & G (Rai 2017, 2018) and IN & NS.

The following is a brief summary of the findings of Rai (2017, 2018). The DNSs of the flat plate wakes show that vortex shedding is vigorous in the low θ/D cases (Cases A and D) and that there is a substantial decrease in shedding intensity as θ/D increases (Cases E, F & G). Shedding intensity here and elsewhere in the article refers to the strength of the vortex as measured by peak spanwise vorticity magnitude and/or related pressure minimum, or peak upwash/downwash generated near/at the wake centerline. A lack of coherence in the spanwise structure of the shed vortices is observed with increasing θ/D. The interaction between the upper and lower DSLs becomes stronger as θ/D is increased. The proximity of the DSLs in the large θ/D cases essentially reduces their ability to roll-up, and contribute to the strength of the newly formed shed vortices. In Case F the shear layers are so close to each other that the roll-up is essentially prevented and the shed vortices form and remain within the shear layer in the near wake. Case G is similar to Case F in these respects.

An initial examination of shedding in Case F via contours of cross-stream velocity at the wake center-plane ((t, z) plane) at a given x location and also the method of Jeong & Hussain (1985, λ_2 criterion) indicated that vortex shedding may be intermittent. Quiescent regions, between regions of shedding activity, both in time and in the z direction were observed. The former are an indication of potential intermittency in the shedding process. However, a closer look at the shedding process, using fluctuations in TE surface vorticity and animations of velocity vectors, showed that vortex shedding is continuous in time although strengthened/weakened during certain periods in Cases F & G. The investigation showed that boundary layer disturbances (streamwise vortices) can increase/decrease vortex shedding intensity. This effect of streamwise vortices on the shed vortices also has implications with regard to shed vortex structure. The shed vortices are enhanced/weakened over the short distances in the z direction over which the influence of the streamwise vortices is felt. Thus this phenomenon is at the same time also a contributor to the finite z-extent of the shed vortices.

The role of boundary layer velocity fluctuations near the TE as a causative agent of large fluctuations in shedding period was examined; it was found that high- and low-speed streaks cause decreases/increases in shedding period, respectively. This also implies that these streaks affect shed

vortex structure; increases/decreases in shedding frequency are obtained over a z-extent that corresponds to the characteristic widths of these streaks, thus contributing to the finite width of the vortices in the z-direction. The effect of increasing the ratio θ/D on centerline velocity spectra and time-averaged, near-wake velocity statistics was also discussed in the two articles.

It is of interest to understand additional changes in near wake behavior as the TE thickness is reduced to values considerably below that of Case G, and all the way to a sharp TE. The wake of the thin flat plate with a sharp TE and turbulent boundary layers has been discussed in several articles, one of the earliest being that of Chevray & Kovasznay (1969). The ratio of the boundary layer momentum thickness to the TE thickness of the plate (θ/D) is large (23.2) in their study. Profiles of measured mean velocity and turbulent normal intensities and shear stress are provided. The boundary layers merge gradually to form the wake. Large-scale vortex shedding is absent. Other notable experimental investigations of the thin flat plate with a sharp trailing edge include those of Andreopoulos & Bradshaw (1980), Ramaprian et al (1982), Nakayama & Liu (1990), Hayakawa & Iida (1992) and Thomas & Liu (2004). In addition to the experimental investigations mentioned above analytical solutions based on simplifying assumptions are provided by Alber (1980). In this study the centerline velocity distribution in the streamwise direction (x) in a region of the near wake is approximated by a logarithmic relation similar in form to that obtained for the turbulent boundary layer upstream of the wake in these cases. A good comparison is obtained between experimental data and the 'wake log-law' in the near wake. Andreopoulos & Bradshaw (1980) observed this logarithmic behavior of the mean velocity in the near wake as well in their experimental data. A brief review of these articles is provided in Rai (2017).

Case ST (Sharp TE) was computed to understand the "Limiting Case" in the series of DNSs undertaken, and two features observed in the experimental investigation of Hayakawa & Iida (1992): 1) The centerline values in normal intensity, and peak value in shear stress profiles in the cross-stream direction (y), were found to first increase in the x direction, from that obtained at the TE, before decreasing further downstream. 2) A broadband peak was observed in centerline cross-stream velocity spectra. The authors attribute the broadband peak to quasi-periodic velocity fluctuations (possibly due to vortices or wave-like motions). They suggest that periodic motion is likely because the velocity profile consists of two shear layers (mean vorticity of opposite sign) and is thus unstable, and that their data indicate the presence of velocity perturbations of the anti-symmetric type, corresponding to sinuous motion of the wake. The question left unanswered is whether the primary contributor to the quasi-periodic fluctuations is wavy motion or vortices. Case ST sheds light on some of the interesting features of the experiment.

In the context of near-wake instability of plates with sharp TEs, it is of interest to visit the early work of Sato & Kuriki (1961) on the transition of the *laminar wake*. The authors, in their experimental investigation, identify three regions of the near wake: 1) The linear region where two-dimensional sinusoidal disturbances are amplified exponentially with increasing x; 2) The non-linear region where two-dimensionality is maintained, but higher harmonics appear and the amplification is no longer exponential; 3) The three-dimensional region where the velocity fluctuations become three-dimensional. Of particular interest is their vortex model with a single row of vortices of alternating sign in the linear region, transitioning to a double row of vortices in the non-linear region, followed by three-dimensional distortion of the vortices in the three-dimensional region. Early stability analyses of the laminar wake are provided in Mattingly & Criminale (1972) and Papageorgougiou & Smith (1989).

In addition to the sharp TE case computed here, it also of interest to understand the intermediate physics leading to this limiting case. The cylinder in a uniform steady ambient flow, for example, does not shed vortices for Reynolds numbers under about 40. Instead, only attached regions of separation or "attached eddies" are observed. At even lower Reynolds (estimated to be around 3.2, Nisi & Porter (1923) even the attached eddies disappear. A review of the early research on low Reynolds number cylinder wakes, is provided by Tritton (1959). The questions that arise with regard to the flat plate wake, resulting from the behavior observed in the cylinder wake, are as follows: Does the flat plate with turbulent separating boundary layers and a circular TE also exhibit attached eddies without vortex shedding

(perhaps not steady, but attached nonetheless)? Are they observed continuously or only occasionally? Do they detach from the surface and form shed vortices intermittently? Do the attached eddies disappear at a sufficiently low Reynolds number as in the cylinder case? If so, what are the representative Reynolds numbers at which these phenomena are observed? Obtaining the answers to these questions is the second objective of the present study. Cases IN (IN stands for Intermittent Shedding) and NS (essentially No Shedding) were computed for this purpose.

In Rai (2018) the analysis of Cases F & G showed the increasing effect of turbulent boundary layer vortices/disturbances on the shedding process when Re_D is decreased. It seemed that further decreases in Re_D would result in intermittent vortex shedding primarily due to the considerable weakening of the already very weak shed vortices by streamwise vortices in the DSLs. As will be seen shortly, Case IN exhibits some rather surprising behavior.

2. FLAT-PLATE COMPUTATIONAL GRID, FLOW/GEOMETRY PARAMETERS AND NUMERICAL METHOD

The computational region for the DNSs of the flat plates with a circular TE is divided into two zones to facilitate grid generation and provide adequate grid resolution for the wake. Figure 1 shows a typical plate cross-section and the two zones that comprise the computational region. The three-dimensional zones and grids are obtained by uniformly spacing copies of these two-dimensional zones in the z direction. The plate zone is bounded by four boundaries: the plate surface (excluding the trailing edge), an external boundary and, two zonal boundaries (top and bottom) that interface with the wake zone. The wake zone is constructed to provide adequate grid resolution for the DSLs, the recirculation region (if any) and the wake. The boundaries of this zone include the circular TE, the upper and lower boundaries and the exit boundary. Both the upper and lower boundaries consist of a zonal boundary segment that interfaces with the plate zone and a second segment that serves as an external boundary. The coordinate system shown in Fig. 1 is only indicative of the coordinate directions; the origin is at the center of the circular TE (as in Fig. 2).

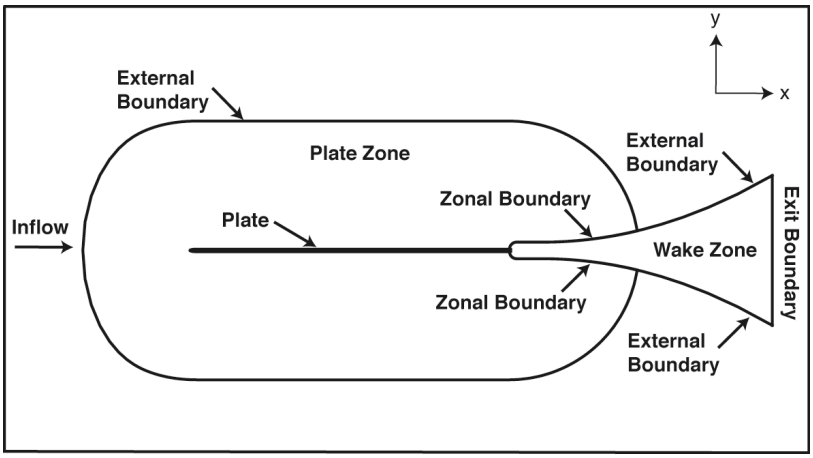

Figure 1. Midspan plate section and multiple zone discretization of the computational region for the circular TE cases (Rai 2013).

The placement of the various boundaries in relation to the plate surface in Cases A & D is provided in Rai (2013, 2014 & 2015). The vertical extent of the wake zone near the TE, where its upper/lower boundaries are horizontal is large enough to completely contain the wake in all cases (Fig. 4 in Rai 2013 clearly shows the adequacy of this dimension in Case A). The spanwise extent of the region in Cases A & D is 4.0D. *Cases A & D are labeled as A & D in Rai (2015) as well.*

Figure 2 shows representative grids in the vicinity of the TE in both zones. Both the grids have the same spacing in the wall normal direction at the plate surface. Downstream of the region of interest ($x/D \approx 13.5$ in Cases A & D and larger x/D values in the other cases), the wake grid coarsens gradually in the x direction. This coarsening reduces computational costs and dissipates the wake to a degree that inviscid exit boundary conditions can be employed at the exit boundary of the wake zone. The wake grid for Case A was constructed with 741 grid points in the streamwise direction, 411 in the cross-stream direction and 256 in the spanwise direction (about 78 x 10^6 grid points). The resolution achieved along the centerline in the three spatial directions at x/D = 10.0 is approximately $\Delta x/\eta = 3.7$, $\Delta y/\eta = 2.2$ and $\Delta z/\eta = 2.1$ where η is the computed Kolmogorov length scale at the same location. The grid resolution in the plate grid in the x, y and z directions for this case is about 17.8, 0.84 and 6.6 wall units respectively, based on the wall shear velocity near the end of the plate. The grid resolution achieved in cases A, D, E, F & G, is similar. The adequacy of the grid resolution and domain size used is demonstrated in Rai (2013 & 2014). The computations are all performed at the same freestream Mach number of 0.2. Compressibility effects are quite small at this Mach number.

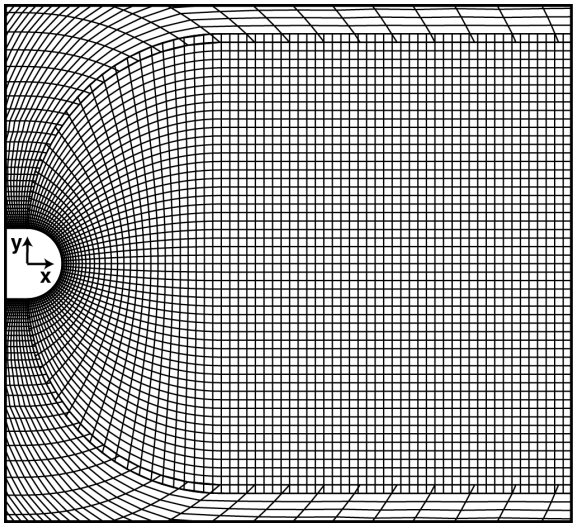

Figure 2. Representative grids in the plate and wake zones in the trailing edge region (Rai 2013).

The primary goal in the current investigation and in Rai (2017 & 2018) is to study the effect of substantially increasing θ/D on various characteristics of the wake. Accordingly, the thickness of the plate in Cases E, F & G was reduced by a factor of 2, 8 & 20, respectively, from that used in Case D. The length of the plate in Cases E, F & G was the same as in Cases A & D. In Cases E, F & G the extent of the computational region in the z direction (Δz) in terms of this constant plate length (L) was kept the same as in Case D to ensure that the computed statistics on the plate were not affected by the imposition of periodicity in the z direction. However, the thickness of the plate was reduced as mentioned earlier. The grid resolution in the z direction is the same as in Case D. For the same reason (an accurate simulation/representation of the separated boundary layer), the vertical extent of the wake region (in the region where the upper and lower boundaries are horizontal) was also maintained at approximately the same value as in Case D. The same reasoning was also used in the placement of the external boundary of the plate zone and the exit boundary of the wake zone in Cases E, F & G. Values of Re_D and the ratio $\psi = (\theta/D)/(\theta/D)_{Case\ A}$ for Cases A, D, E, F & G were provided in Table 1. The Reynolds number based on plate length L is the same in all cases, $Re_L = 1.25 \times 10^6$.

The computational domains for Cases IN & NS were obtained using the same principles as in Cases E, F & G. The z-extent of the computational domain and the grid resolution used in this direction are the same as in Cases E, F and G. However, the grid resolution in the (x, y) plane in the TE region is

much finer in order to resolve the geometry and flow in this region. The resolution in the (x, y) plane in the TE region is significantly more than required for the upstream turbulent boundary layer of the plate (less than about 0.25 wall units in the wall-tangential/normal directions in Case IN, even finer in Case NS).

Case ST was computed on a simple single "C-Grid". Figure 3 shows the grid in the TE region. The streamwise and cross-stream coordinates are normalized using the plate thickness (H_{ST}) upstream of the tapered region (same as the plate thickness in Case F). The figure also shows the plate surface and the TE (barely discernible from the grid). Here again, as in Cases IN and NS, the streamwise resolution near the trailing edge is substantially more than required for computing the upstream turbulent boundary layer (less than one wall unit). This choice was made to very accurately compute any initial interaction between the upper and lower separated boundary layers. The grid then coarsens gradually in the x and y directions. The domain size and resolution used in the z direction is the same as in Cases IN & NS. A simple "C" and vertical exit boundary comprise the external boundaries in this case.

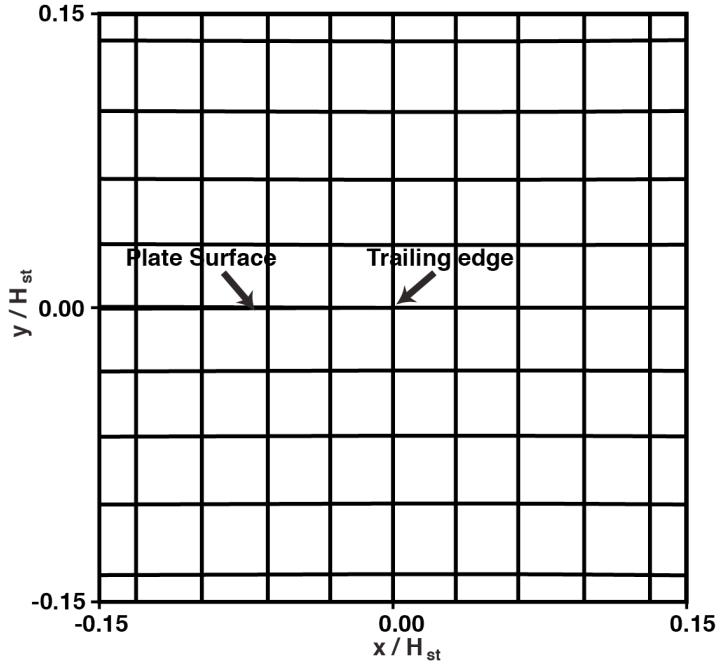

Figure 3. Grid in the TE region for Case ST.

A high-order accurate upwind-biased method is used here to compute the flow over the plate as well as that in the wake. The convective terms are computed using sixth- and seventh-order upwind-biased finite differences, both with seventh-order dissipation terms. These dissipation terms are the naturally occurring truncation error terms that are obtained in the upwind-biased finite-difference approximation to the convective terms. The viscous terms are computed with fourth-order central differences. The method is iterative-implicit in nature, multiple iterations are employed at each time-step to solve the nonlinear finite-difference equations arising from a fully implicit formulation; the method is second-order accurate in time. The boundaries that contain the computational grids can be classified as natural and zonal boundaries in the circular TE case. The natural boundaries include the external boundary of the plate grid, the surface of the plate, the exit boundary of the wake grid, the segments of the upper and lower boundaries of the wake grid labeled as "external boundary" in Fig. 1, and, the boundaries in the *z* direction. The upstream segment of the upper boundary between the plate and wake grids is an example of the zonal boundaries used in the computation. Periodic boundary conditions are imposed on the boundaries in the *z* direction (homogeneity in *z*). No-slip/adiabatic wall conditions are used on the plate surface. Wall blowing/suction is implemented on a short segment on both the upper and lower surfaces of the plate to induce transition to turbulence. The boundary layer is turbulent well

upstream of the trailing edge. The upper and lower transitional/turbulent boundary layers and the wake are all computed via DNS. The natural and zonal boundary conditions, and the high-order accurate upwind-biased finite-difference method used here are discussed in detail in the present author's earlier articles cited in Rai (2015). The natural boundary conditions used in Case ST are the same as in the circular TE cases, however, there are no zonal boundaries because a single "C" grid is used in this case.

A discussion of the adequacy of the resolution used in the computations presented here via comparisons of DNS data obtained using the present method with 1) experimental cylinder wake data (Ong, Wallace & Moin, 1995) and 2) boundary layer data (Karlsson & Johansson, 1988) is provided in Rai (2017). An extensive comparison of the DNS data obtained for fully developed turbulent channel flow with an earlier version of the present method (lower-order of spatial accuracy for the inviscid terms, Rai & Moin 1991) and spectral method data (Kim Moin & Moser, 1987) is also discussed in Rai (2017). These comparisons demonstrate the adequacy of the grid resolution used in the plate and wake grids. The adequacy of the size of the computational domain in all three spatial directions is also discussed at some length in Rai (2017). In the interest of brevity these discussions have been omitted in the present article.

3. CHARACTERISTICS OF THE NEAR-WAKE IN CASES ST, NS & IN

The data provided in the following figures were obtained during the data-sampling period (after the initial transients were eliminated). In the following contour plots the colors blue/green represent negative values (deep blue representing the lowest value) of the term/quantity being discussed. Orange, red and magenta represent positive values (magenta bordering on white representing the highest value). Shades of yellow represent values close to zero.

3.1 Case ST

Hayakawa & Iida (1992) obtained flat plate wake data with a sharp trailing edge (0.2mm) to investigate the very near wake ($x^+ < 500$, here the streamwise distance x is normalized by the wall shear velocity and kinematic viscosity near the TE). The centerline values in normal intensity and peak value in shear stress profiles in the cross-stream direction were found to first increase with increasing x, from that obtained at the TE, before decreasing further downstream. Based on space-time correlations, the authors attribute the initial increase in intensities and shear stress to an interaction between wall turbulence from either side of the plate upon merger at the TE, and a change in orientation of longitudinal vortices. Of particular interest is a broadband peak obtained in centerline cross-stream velocity spectra, indicating quasi-periodicity (possibly due to vortices or wave-like motions). Case ST in the present investigation was computed to, among other things, obtain a better understanding of these phenomena (broadband peak & increase in intensity levels) and also to obtain computational evidence for the presence/absence of the sinuous motion of the inner wake and near-centerline vortices hypothesized by Hayakawa & Iida (1992). Case ST also represents the 'Limiting Case' in the sequence of computations with decreasing TE diameter (Cases F, G, IN, NS) performed by the present author.

Figure 4 showing contours of instantaneous spanwise velocity in the TE region for Case ST is provided as an introduction to the near-wake of the flat plate with a sharp TE. Spanwise velocity fluctuations are an excellent indicator of the three-dimensionality of the turbulent boundary layers and wake where the mean flow is two-dimensional. The upper and lower turbulent boundary layers, their smooth merger past the trailing edge, and the initial development of the turbulent wake are all observed in Fig. 4. As expected shedding is absent in this case (confirmed via animations of velocity vectors).

We next investigate the behavior of the upper & lower DSLs. Figure 5 shows contours of instantaneous spanwise vorticity in a (x, y) plane in the near wake for Case ST. While some sinuous motion of the inner wake is apparent for $x / H_{ST} < 6.0$, the dominant feature in this figure is the set of spanwise vortices (for the most part of alternating sign). They are seen as regions of clustered contours

with a peak within both the DSLs, in the range -1.0 < y / H_{ST} < 1.0, for x / H_{ST} < 6.0. Further downstream these nascent vortices evolve into well-developed spanwise vortices (labeled A, B & C). Contours of streamwise vorticity show that A, B & C possess a streamwise component as well. This behavior is reminiscent of the instability of the DSLs that is observed in the thick flat plate Cases of Rai (2014 & 2015). The question that arises is as follows: Is this a rare phenomenon or does it occur repeatedly?

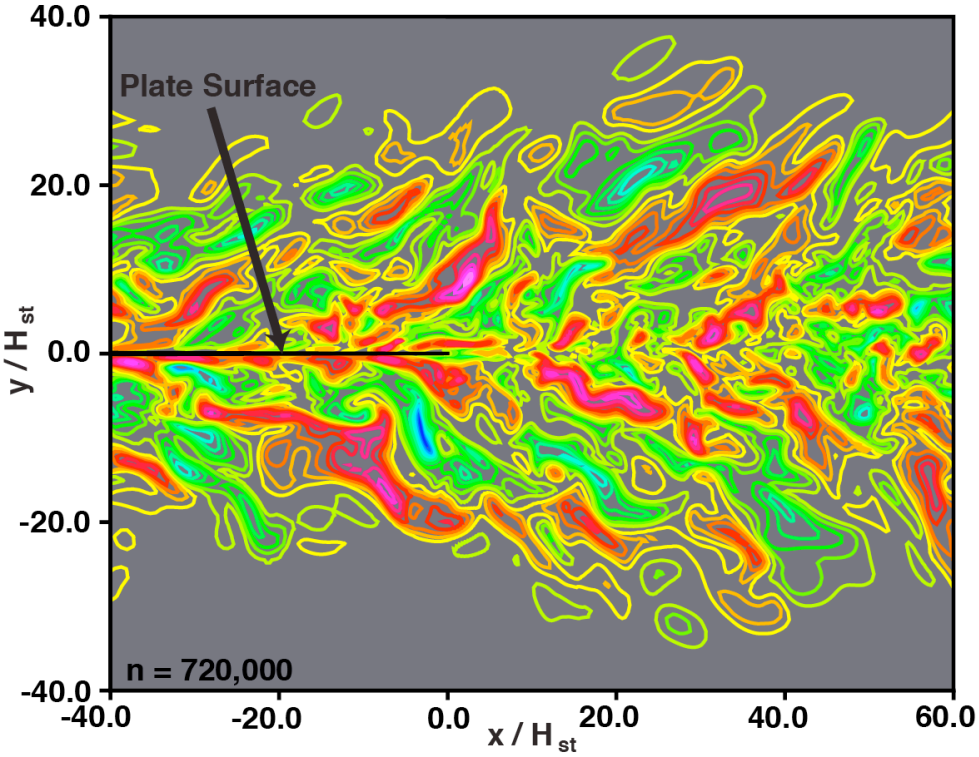

Fig. 4. Contours of instantaneous spanwise velocity in a (x, y) plane, Case ST.

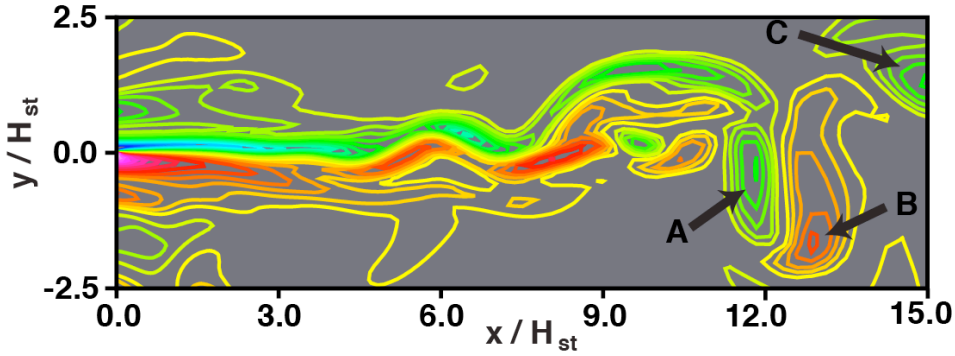

Fig. 5. Contours of instantaneous spanwise vorticity in a (x, y) plane (Event B, see Fig. 6), Case ST.

Figure 6 shows contours of cross-stream velocity (*v*) as a function of time and z (in a (t, z) plane) at x / H_{st} = 6.0, y / H_{st} = 0.0. Similar plots (utilizing fluctuating pressure, streamwise and cross-stream velocity components were used effectively in Rai (2010, 2015, 2017 & 2018) to study both shear layer vortices and shed vortices. The passage of shed vortices and shear layer vortices (largely spanwise vortices) past a given point results in alternating bands of opposite sign of the quantity of interest (blue/red, in this case *v*). Such pairs of bands (in some cases multiple pairs) are observed in Fig. 6. Five different regions (events) from Fig. 6 were identified for further study. They are marked with rectangles. All of them showed a near-wake instability of the type seen in Fig. 5. Clearly the wake instability of Fig. 5 is

not an infrequent occurrence. It is a dominant feature of the near wake in Case ST. Unlike the thin plate cases F & G discussed at length in Rai (2017 & 2018) where the shed vortices first form by about x/D = 1.5, here the wake instability generally manifests further downstream (hence the choice of $x / H_{st} = 6.0$ instead of a location further upstream). The spanwise vortices of Fig. 5 were confirmed using both the λ_2 criterion of Jeong & Hussain (1995) and instantaneous velocity vectors; circulating flow was evident after subtracting the velocity at the center of the candidate vortex. These two tests were also performed for the vortices of the different events identified in Fig. 6.

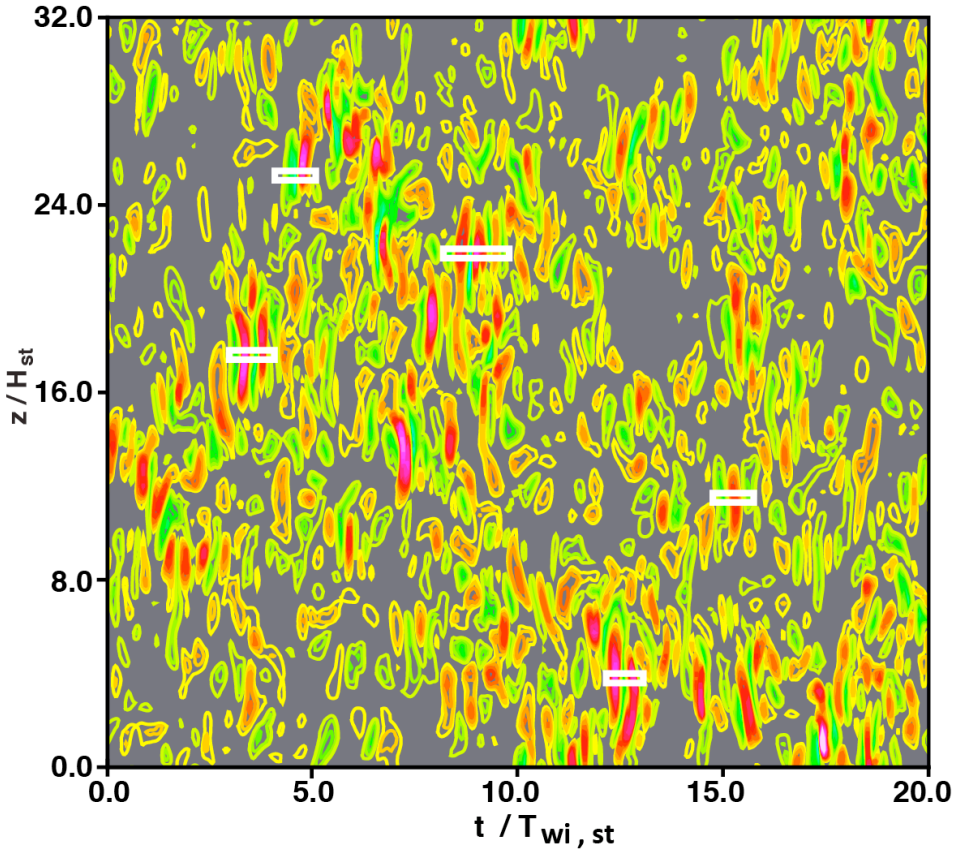

Fig. 6. Contours of *v* in a (t, z) plane at $x / H_{st} = 6.0$, $y / H_{st} = 0.0$, Case ST.

This finding leads to the expectation of a broadband peak in the spectrum obtained for *v* at the location $x / H_{st} = 6.0$, $y / H_{st} = 0.0$. Figure 7 shows this spectrum. The broadband peak is evident. The frequency ω is normalized by $\omega_{wi,\ Case\ ST}$, the frequency at which the peak occurs (this is the frequency that characterizes the instability). The peak is in accordance with the finding of Hayakawa and Iida (1992) except that we have identified the source to be largely spanwise vortices associated with a near wake instability. Of interest is that Fig. 5 shows both positive and negative spanwise vortices, that is, both the upper and lower DSLs exhibit the instability. An analysis of the events marked in Fig. 6 show that the instability related wake vortices are not always of approximately the same strength and size at a given x location; the instability can be more pronounced on the upper or lower sides of the central wake region (characterized by negative/positive DSL related vorticity, respectively). In addition, the intensity of the wake instability can vary significantly between instability events. The instability frequency ($\omega_{wi,\ Case\ ST}$) of the wake in Case ST is only about 15% higher than the DSL instability frequency obtained in Case A (boundary layer properties upstream of the separation point are roughly the same in Cases A and ST).

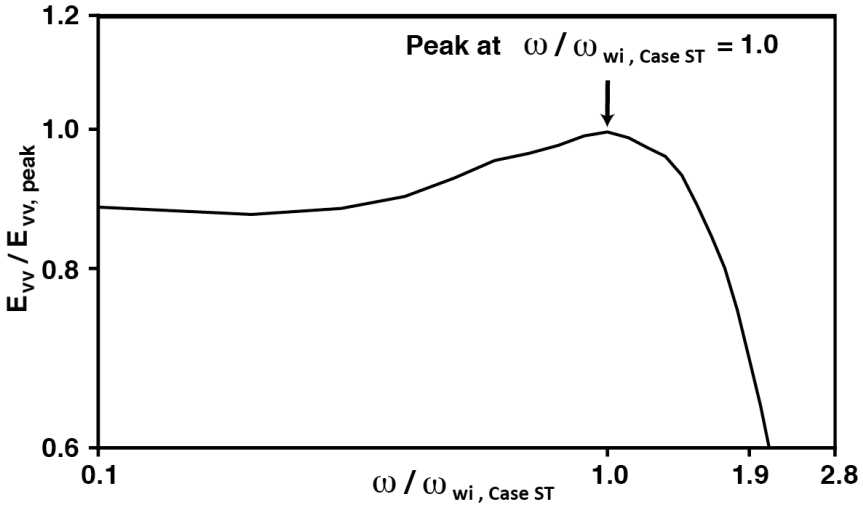

Figure 7. Spectrum obtained for *v* in Case ST (x / H_{st} = 6.0, y / H_{st} = 0.0).

The near wake instability seen here is reminiscent of the one investigated in Sato & Kuriki (1961, S&K), described earlier in the introduction. However, they are different; here we have the instability of two merging *turbulent* DSLs, in S&K the instability was associated with two merging *laminar* DSLs. The near-wake streamwise velocity (*u*) profiles in the y direction are substantially different in the two cases; the minimum in the centerline *u* profile observed in S&K is absent in the present case (continually increasing *u* with increasing x in Case ST). In addition the continuous sinusoidal waveforms observed in S&K, in the inner region, are the effect of acoustic disturbances introduced to make the instability phenomenon more robust. Here, log-layer eddies (found both in the boundary layer prior to separation and downstream of the TE) are one probable cause of instability initiation (this was identified as one of the shear-layer-vortex-initiating causes in the case of the DSL of a thick flat plate in Rai 2015). However, it is interesting that the near wake in the laminar *and* turbulent cases exhibits unstable behavior.

It is of interest to distinguish between periods of wake instability and periods of calm. Figure 8 shows contours of instantaneous spanwise vorticity from a quiet period in Fig. 6. The DSLs are generally unperturbed until about x / H_{st} = 12.0 (in comparison to Fig. 5). Figures 6 & 8 indicate that the wake instability is *intermittent*. The bands in Fig. 6 also show that the wake instability is of finite extent in the z direction (similar to the DSL instability); the bands are between 1.0H_{ST} and 3.0H_{ST} in z-extent.

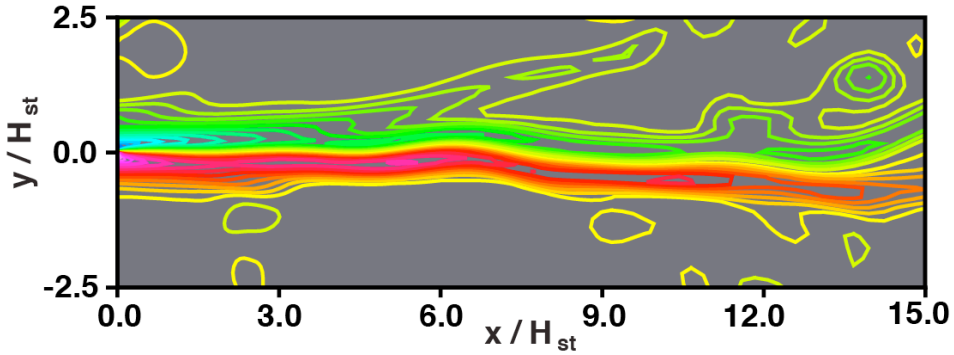

Figure 8. Contours of instantaneous spanwise vorticity in a (x, y) plane, Case ST.

As in Hayakawa & Iida (1992) the centerline values in normal intensity and the peak value in shear stress profiles in the y direction, were found to initially increase with increasing x from that obtained at the TE in Case ST, before decreasing further downstream. The spanwise vortices of Fig. 5 would certainly contribute to the increase in centerline cross-stream intensity; the centerline maximum occurs at

x / H_{st} = 17.4 in Case ST (just downstream of the right boundary of Fig. 5 where the vortices are well formed). Displacement of the spanwise vortices away from the centerline (also observed in Fig. 5) would contribute to the streamwise intensity at the centerline. Finally, the streamwise vorticity component in the largely spanwise vortices would contribute to the centerline cross-stream and spanwise intensity values. The increase in the peak in shear stress profiles is likely related to the increases in streamwise and cross-stream intensities. In the experiment, detailed measurements were made at the Reynolds numbers Re_θ = 800, 1100 (measured at the TE). Case ST was mainly computed as the limiting case in a series of computations (Table 1) and thus has the same plate length as in the other computations and a larger value of Re_θ than in the experiment. Despite the difference in Reynolds numbers the reasons underlying the interesting flow features of the experiment are most likely the same as in the computation.

3.2 Case NS

Given the sequence of computations (Cases A, D, E, F & G with decreasing plate thickness) it would seem natural to first discuss Case IN before Case NS. However, because near-wake behavior is simpler in Case NS than in Case IN (Case IN exhibits the additional feature of intermittent vortex shedding), the two are discussed in 'reverse order'. As in Cases F, G and ST, contours of *v* in a (t, z) plane (at x/D = 1.0, y/D = 0.0) were examined. Figure 9 shows these contours and seven events of interest with positive/negative bands that in Cases F & G were signatures of shed vortices. The z coordinate has been normalized with H_{st} instead of the TE diameter of Case NS so that Figs. 6 and 9 can be compared easily. While the two figures are qualitatively similar (clustered bands with quiescent regions in between) the reasons underlying the appearance of the bands is very different in the two cases.

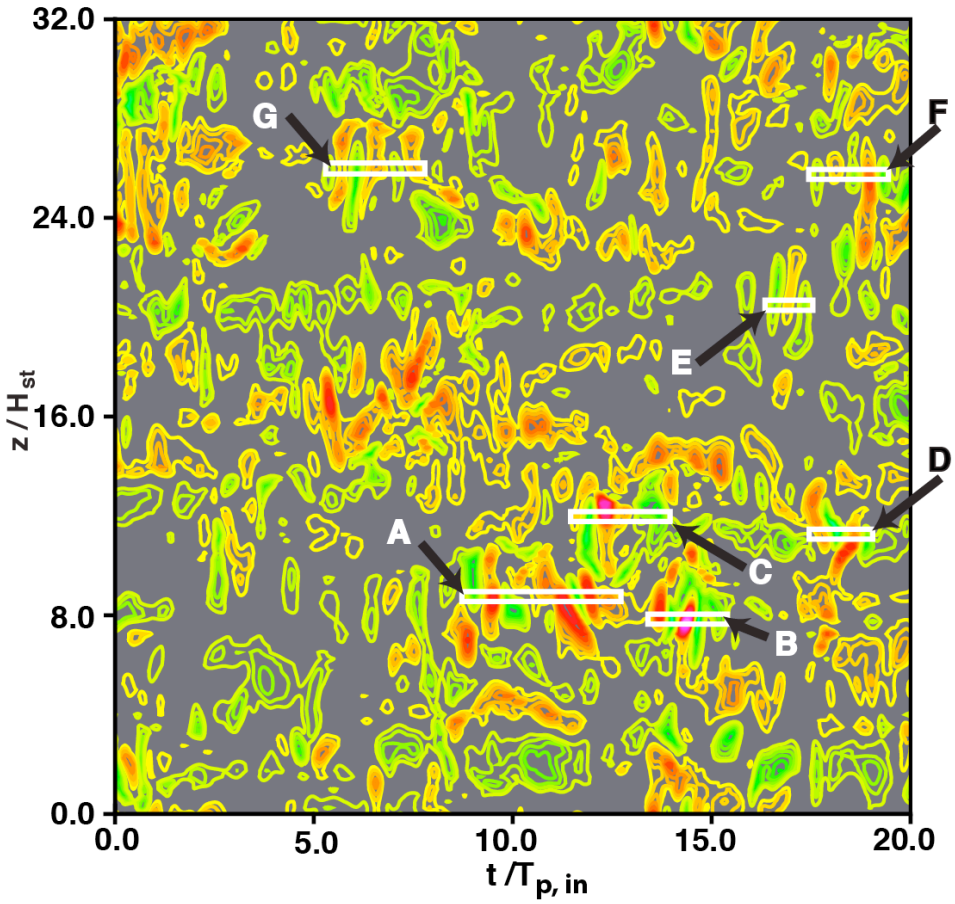

Fig. 9. Contours of *v* in a (t, z) plane at x/D = 1.0, y/D = 0.0, Case NS.

Figure 10 shows stream traces obtained with instantaneous velocity fields at four different instants within Event B (Fig. 9). Stream traces are used in Case NS (instead of instantaneous velocity vectors) because of large variations in velocity vector magnitudes (visualizing the smallest and the largest vectors simultaneously, with clarity, in a single plot is difficult). Clearly there is no evidence of a region of separation (attached eddy) or shed vortex in any of the sub-plots. An animation of the entire event (B) also showed no sign of a shed vortex or the formation of an attached region of separation. However, the flow exhibits large variations in flow direction. The upward and downward flow directions are evident in Fig.10. The changes in direction are seen as alternating positive/negative bands in Fig. 9. All of the events (A – G) were investigated similarly. Except for Event D none of them showed an attached eddy or shed vortex. Only Event D showed the formation of a single vortex (preceded by a single short-lived attached eddy). The initiation of the observed shedding of this one vortex is similar to that encountered in Case IN and for that reason the process is discussed in the next sub-section.

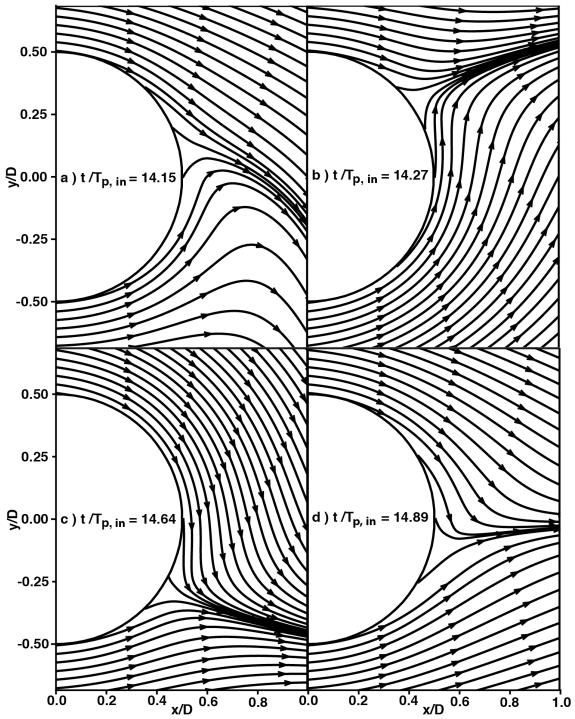

Fig. 10. Stream traces at 4 time instants obtained using instantaneous velocity fields, Event B, Case NS.

One objective of the investigation by Rai (2018) was to determine the important contributors to the variability in the strength of shed vortices. Accordingly the data obtained in Case F was analyzed extensively with the aid of the vorticity transport equation for spanwise vorticity. The analysis showed that streamwise vortices in the DSLs that are in proximity to the shed vortices play a critical role in both strengthening and weakening shed vortices in the wake. The mechanism involves the generation of high levels of the gradient of the spanwise velocity in the z direction ($\partial w/\partial z$) which then interacts with the spanwise vorticity associated with the DSLs to yield regions which either strengthen (positive $\partial w/\partial z$) or weaken (negative $\partial w/\partial z$) shed vortices. Here again we investigate the possible role of streamwise vortices in the DSLs in creating upward/downward motion in the TE region (as in Fig. 10).

Figure 11 shows contours of instantaneous streamwise vorticity in an end-plane (constant x, x/D = 1.0, view from a point downstream). The time instant corresponds to Fig. 10a. The y extent is sufficiently large to depict the streamwise vortices of interest and, the z-extent spans Event B. The three streamwise vortices of interest are labeled as A, B & C. Region S is not a vortex (λ_2 criterion of Jeong & Hussain (1995)). Figure 12 shows instantaneous velocity vectors (w, v) overlaid on the streamwise

vorticity contours. The circulating flow induced by vortices A & C is easily observed. Vortex B is weaker and thus its induced flow is not apparent. Subtracting the velocity vector at its center from the velocity vector field does show weakly circulating flow. The region contained within the rectangle contains the z location of event B and the y extent of interest (from Fig. 10a). The downward component of the flow in this region is largely induced by vortices A & B. Upward/downward flow can also be induced by occasional spanwise vortices in the DSLs (originating in the upstream turbulent boundary layer). Thus turbulent vortices and other features of the turbulent boundary layer that subsequently become a part of the DSLs cause the oscillations in the flow direction in the TE region. As will be seen in Case IN, these oscillations sometimes initiate the shedding of vortices. The very low Reynolds number associated with Case NS essentially prevents near surface separation of flow in the TE region and thus the subsequent formation of both attached eddies and shed vortices. Case NS is *essentially* a non-shedding case.

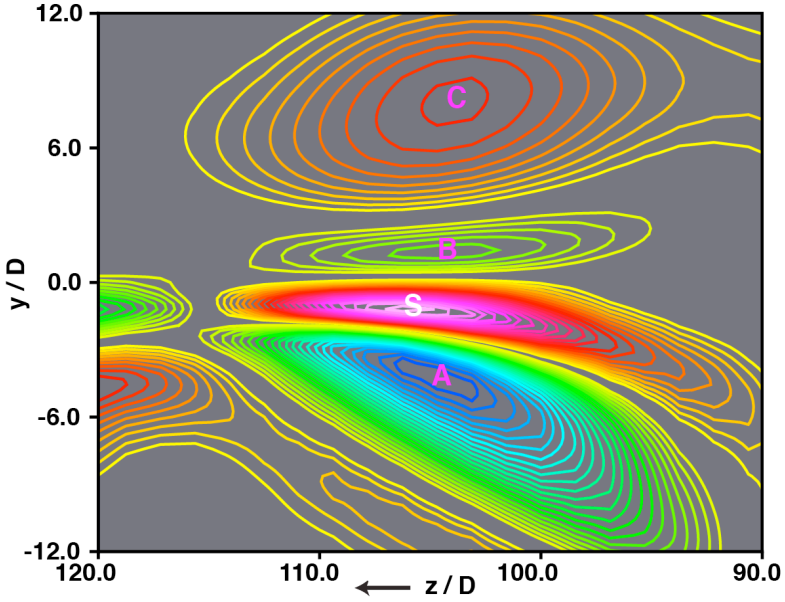

Fig. 11. Contours of instantaneous streamwise vorticity in an end-plane at x/D = 1.0, Case NS.

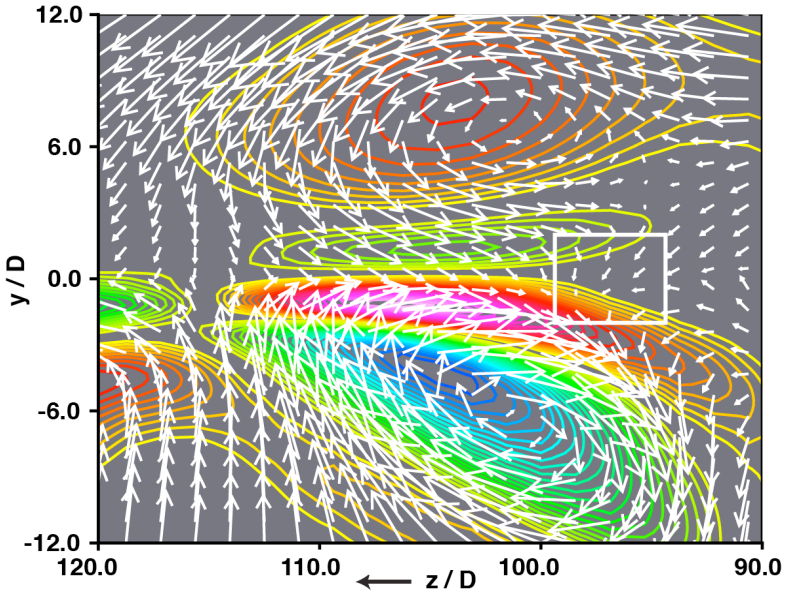

Fig. 12. Instantaneous velocity vectors superimposed on contours of instantaneous streamwise vorticity in an end-plane at x/D = 1.0, Case NS.

3.3 Case IN

In Rai (2018) the analysis of Cases F & G clearly showed the increasing effect of turbulent boundary layer vortices/disturbances on the shedding process when Re_D is decreased. It seemed that further decreases in Re_D may result in intermittent vortex shedding primarily due to the occasional weakening of the already very weak shed vortices, by streamwise vortices in the DSLs. Surprisingly, in Case IN, the oscillations in flow direction in the TE region, *caused by disturbances related to turbulence in the DSLs*, sometimes results in short periods of intermittent shedding. Despite this surprising behavior that is somewhat counter-intuitive, there is still the possibility of turbulent vortices weakening shed vortices to an extent that shedding intermittency is observed as the Reynolds number is decreased from that of Case G (continuous shedding, Rai 2018). The Reynolds number at which this *possible second type of intermittency* may occur has not yet been determined. Intermittent shedding, as observed in Case IN, is discussed below.

Figure 13 shows contours of *v* in a (t, z) plane over a time-period corresponding to 20 shedding periods at x/D = 1.0, y/D = 0.0. The concept of the shedding period, that is very intuitive when shedding is continuous, is somewhat nebulous here given that at times only one or two vortices are shed (more at other times). Here the shedding period is obtained from the *v* spectrum computed at x/D = 1.0, y/D = 0.0. As in Cases ST & NS, events of interest are marked with rectangles. The white rectangles encompass regions where the TE flow is primarily either upward or downward (no change in general direction). The black rectangles contain regions with multiple pairs of alternating positive/negative bands of *v* that signal the possible presence of shed vortices.

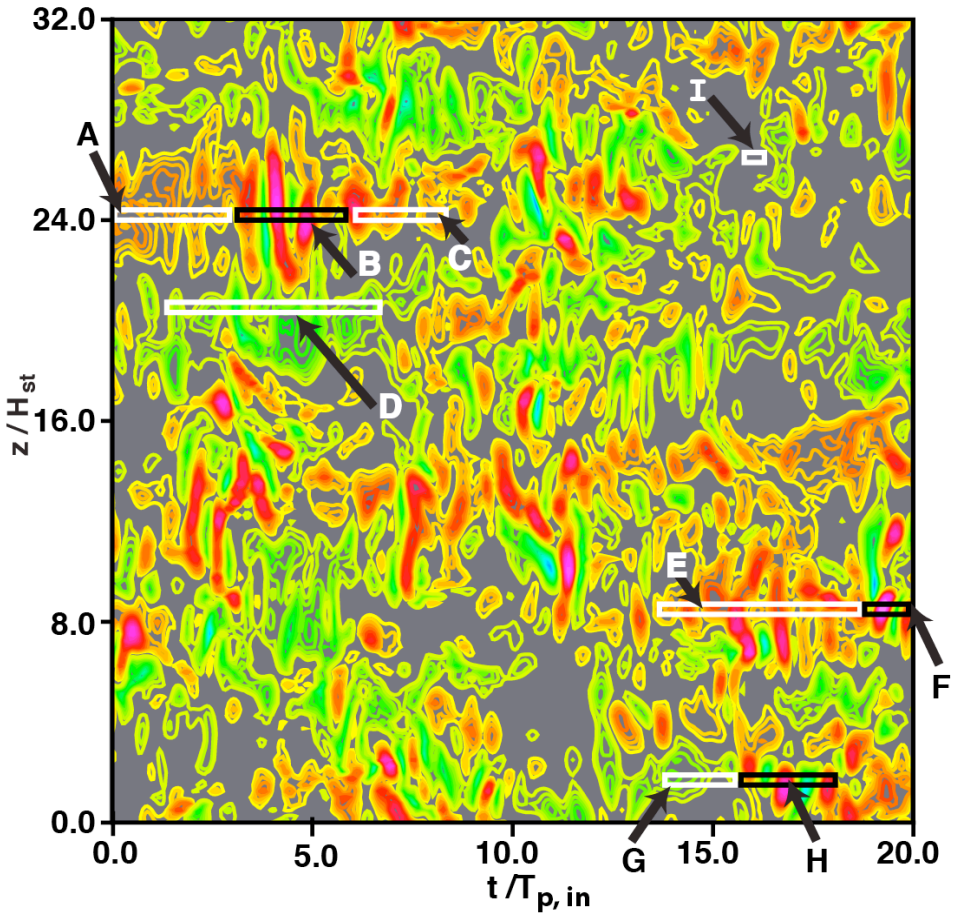

Fig. 13. Contours of *v* at x/D = 1.0, y/D = 0.0 over 20 shedding periods, Case IN.

Event D is populated largely by negative values of *v*. An animation of velocity vectors and stream traces in a (x, y) plane containing the TE region showed no evidence of shed vortices. The base flow was downward during the entire period. Similarly, shed vortices were absent in Events A, C & E. The TE flow was upward during these three periods. Events B and F both clearly showed the initiation of vortex shedding. Initiation occurred when the flow direction changed rapidly from upward to downward.

Figure 14 shows instantaneous velocity vectors in a (x, y) plane at the beginning of Event F. The flow is initially upward (Fig. 14a); this instant is at the end of Region E (red/positive *v*). Several features of interest are observed in the following figure, Fig. 14b. Both the *v* component and the velocity magnitude in the lower right corner are reduced compared to that observed in Fig. 14a; this indicates that the causative agent for the upward TE flow has a diminished effect at the time instant of Fig. 14b. The velocity is also reduced in the regions that are highlighted by the arrows labeled A. In fact the near surface flow is almost stagnant. Interestingly the near surface flow in the region marked B continues largely unabated. It seems that the diminishing effect of the causative agent has not yet fully reached this area.

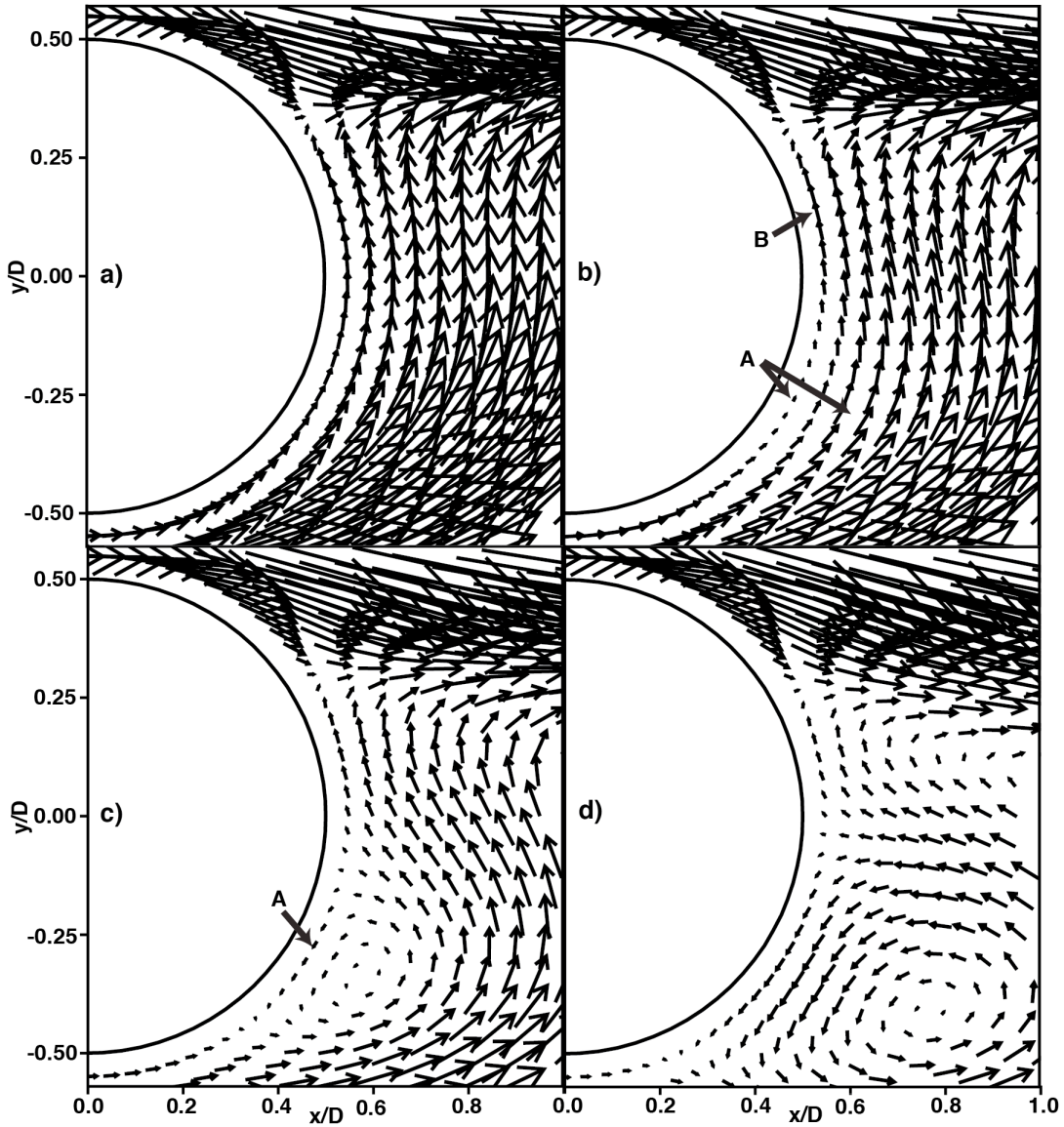

Fig. 14. Instantaneous velocity vectors at different stages of shed-vortex development, Case IN.

Figure 14c shows the first appearance of reverse flow in the near surface region (see arrow); it causes the flow to circulate. This of course is the classical shedding mechanism; the low momentum near-surface-flow is unable to overcome the adverse pressure gradient whereas the higher momentum flow further away from the surface continues in the original direction leading to a separated flow region and subsequently the generation of shed vortices. Figure 14c also shows a continued diminishing of the effect of the causative agent for the original upward flow. Figure 14d shows both a strengthening of the shed vortex and its movement downstream. This process of vortex-shedding *initiation* was found in the other vortex-initiation cases investigated. The shedding of subsequent vortices within a given shedding event may be relatively straightforward as described in Rai (2017), or considerably more complex involving the flow induced by the previous shed vortex as well as the next causative agent for upward/downward flow.

The Event labeled **I** in Fig. 13 is a becalmed region. It is of importance because it sheds light on the nature of the TE flow when the causative agents for oscillating flow direction are weak or temporarily absent. Figure 15a shows instantaneous velocity vectors at a point in time during this event. The flow above the centerline is almost a mirror image of that below the centerline (u is symmetric and v is anti-symmetric). Figure 15b is an enlarged view of the region contained within the rectangle in Fig. 15a. The two attached eddies, one above and one below the centerline, are clearly observed. The flow along the centerline has a near-zero v component of velocity; reverse flow is observed for x/D < 0.865. The computed *mean flow* in the TE region (plot not included here) is very similar to that seen in Figure 15. The event marked G also showed instants in time when the flow was similar to that seen in Fig. 15. Event H, although populated by alternating positive/negative bands, did not show any vortex shedding, thus demonstrating that even at the higher Reynolds number of Case IN (compared to Case NS) significant changes in the direction of TE flow at times does not produce shed vortices (this is similar to the behavior seen in Case NS).

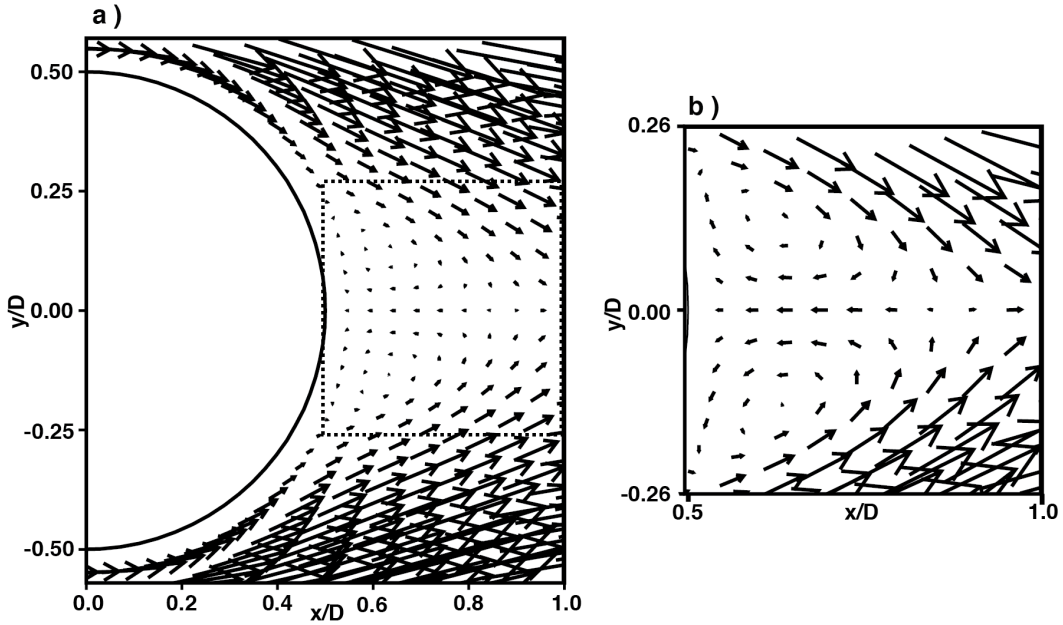

Fig. 15. Instantaneous velocity vectors showing upper/lower attached regions of circulating flow adjacent to the base, Region **I**, Case IN.

Figure 16 shows the spectrum obtained for v at x/D =1.0, y/D = 0.0 in Cases IN and NS. Even though shedding is intermittent in Case IN, the corresponding spectrum does show a peak. The frequency associated with the peak characterizes the intermittent shedding of Case IN. The related shedding period ($T_{p,in}$) is used to normalize time in Fig. 13. As expected the spectrum obtained in Case NS does not

exhibit a peak (for this reason, time is normalized using $T_{p,in}$ in Fig. 9 as well). However, except for the lack of a peak, the spectrum obtained in Case NS resembles that of Case IN.

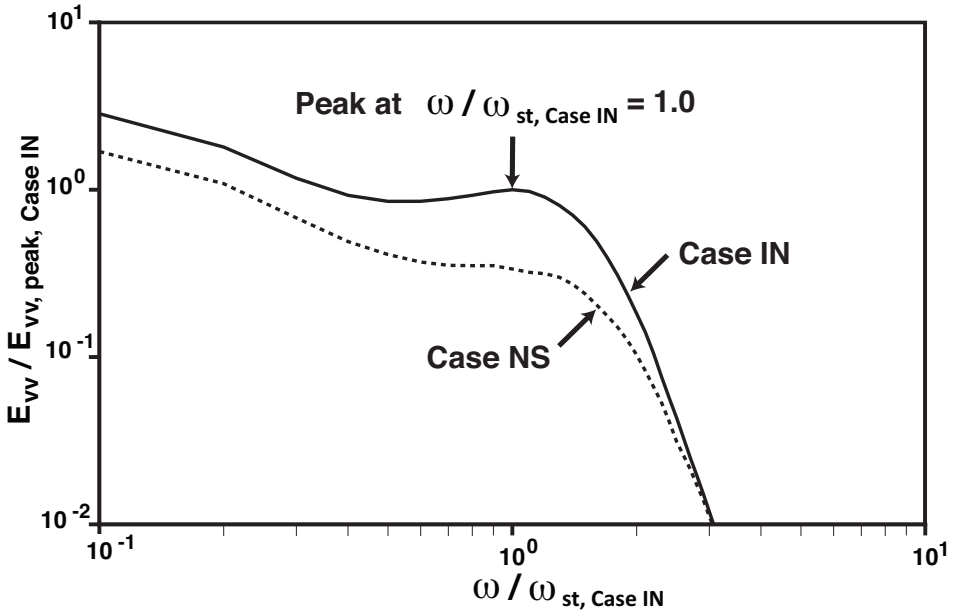

Fig. 16. Comparison of *v* spectrum obtained in Cases IN & NS, x/D = 1.0, y/D = 0.0.

4. CONCLUDING REMARKS

The near and very near wake of thin flat plates with both sharp and circular trailing edges are investigated with direct numerical simulations. The TE is circular in two of the cases (IN & NS) and sharp in one of them (ST). The separating boundary layers are turbulent in all cases. The focus of this study is to explore the effect of significantly reducing Re_D on the near wake.

One of the objectives in Case ST is to understand the reasons underlying the experimental findings of Hayakawa & Iida (1992); that is, the centerline values in normal intensity and the peak in shear stress profiles in the y direction were found to first increase in the x direction, from that obtained at the TE, before decreasing further downstream. In addition a broadband peak was obtained in centerline cross-stream velocity spectra, indicating quasi-periodicity (possibly due to vortices or wave-like motions). These features were observed in the computation (Case ST) as well. Case ST showed a near wake instability resulting in spanwise vortices near the wake centerline (with at times a streamwise component). The instability is intermittent but occurs frequently and is sufficiently powerful to cause a broadband peak in the *v* spectrum (as in the experiment). The instability related vortices are also contributors to the initial increase in centerline normal intensity values in Case ST and very likely in the experiment as well. Case ST is also the “Limiting Case” in the series of DNSs performed; as expected TE vortex shedding was not observed.

Case NS, with the lowest value of Re_D computed thus far (with a circular TE), is an essentially non-shedding case; only one shed vortex was observed (over a time period corresponding to 20 shedding periods of Case IN). The TE flow exhibited oscillations in the direction of motion (upward/downward) as a result of disturbances in the DSLs (vortices and other flow features). The *v* spectrum at x/D = 1.0 did not exhibit a peak despite the oscillating flow direction. Case NS is the flat plate equivalent of the extremely low Reynolds number cylinder cases where attached eddies and vortex shedding are both absent. However, these flow features essentially cease to exist at a much higher Reynolds number (Re_D = 50.0)

in Case NS, than in the case of the cylinder. This suggests that in general, in the case of the flat plate with turbulent separating boundary layers, shedding/attached-eddies disappear earlier (with decreasing values of Re_D) than in the cylinder wake. There is of course the dependence on the momentum thickness of the separating boundary layer; a thinner boundary layer than in Case NS (shorter plate) will likely require a smaller value of Re_D ($Re_D < 50.0$) to obtain a wake that does not shed vortices or exhibit attached eddies.

Case IN, also with a circular trailing edge but twice the value of Re_D as in Case NS, exhibits intermittent shedding. Shedding was initiated when the TE flow direction changed rapidly *due to turbulence*. Calm periods in Case IN resulted in TE flow with two attached eddies much like low Reynolds number cylinder flow. The resulting flow pattern is very similar to that obtained for the computed mean flow in Case IN. Unlike Case NS, Case IN shows a shedding related peak in the *v* spectrum.

The velocity profile along the centerline does not exhibit a region of reverse flow in Cases ST (as expected) and NS; it does show a small region of reverse flow in Case IN.

REFERENCES

ALBER, I. E. 1980 Turbulent wake of a thin, flat plate. *AIAA Journal*, Vol. 18 (9), 1044.

ANDREOPOULOS J. & BRADSHAW, P. 1980 Measurements of interacting turbulent shear layers in the near wake of a flat plate. *Journal of Fluid Mechanics*, Vol. 100, 639.

CHEVRAY, R. & KOVASZNAY, L. S. G. 1969 Turbulence measurements in the wake of a thin flat plate. *AIAA Journal*, Vol. 7, 1641.

HAYAKAWA, M. & Iida, S. –I. 1992 Behavior of turbulence in the near wake of a flat plate at low Reynolds number. *Physics of Fluids A*, Vol. 4 (10) 2282.

JEONG, J. & HUSSAIN, F. 1995 On the identification of a vortex. *Journal of Fluid Mechanics*, Vol. 285, 69.

KARLSSON, R. I. & JOHANSSON, T. G. 1988 LDV Measurements of higher-order moments of velocity fluctuations in a turbulent boundary layer. Laser Anemometry in Fluid Mechanics, Ladoan-Instituto Superior Tecnico, Portugal, 273.

KIM, J., MOIN, P. & MOSER, R. 1987 Turbulence statistics in fully developed channel flow at low Reynolds number. *Journal of Fluid Mechanics,* Vol. 177, 133.

MATTINGLY, G. E. & CRIMINALE, W. O. 1972 The stability of an incompressible two-dimensional wake. *Journal of Fluid Mechanics,* Vol. 51, 232.

ONG, L., WALLACE, J., & MOIN, P. 1995 The velocity and vorticity fields of the turbulent near wake of a circular cylinder. NASA TM -110513.

NAKAYAMA, A. & LIU, B. 1990 The turbulent near wake of a flat plate at low Reynolds number. *Journal of Fluid Mechanics*, Vol. 217, 93.

NISI, H. & PORTER, A. W. 1923 On eddies in air. *The London, Edinburgh, and Dublin Philosophical Magazine and Journal of Science*, Vol. 46, 754.

PAPAGEORGIOU, D. T. & SMITH, F. T. 1989 Linear instability of the wake behind a flat plate placed parallel to a uniform stream. *Journal of Fluid Mechanics*, Vol. 208, 67.

RAI, M. M., & MOIN, P. 1991 Direct simulations of turbulent flow using finite-difference schemes. *Journal of Computational Physics* Vol. 96 (1), 15.

RAI, M. M. 2010 A computational investigation of the instability of the detached shear layers in the wake of a circular cylinder. *Journal of Fluid Mechanics*, Vol. 659, 375.

RAI, M. M. 2013 Flow physics in the turbulent near wake of a flat plate. *Journal of Fluid Mechanics*, Vol. 724, 704.

RAI, M. M. 2014 Flow Phenomena in the very near wake of a flat plate with a circular trailing edge. *Journal of Fluid Mechanics*, Volume 756, 510.

RAI, M. M. 2015 Detached shear-layer instability and entrainment in the wake of a flat plate with turbulent separating boundary layers. *Journal of Fluid Mechanics*, Vol. 774, 5.

RAI, M. M. 2017 Changes in flat plate wake characteristics obtained with decreasing plate thickness. *International Journal of Heat and Fluid Flow*, Vol. 68, 13.

RAI, M. M. 2018 Vortex Shedding Characteristics of the Wake of a Thin Flat Plate With a Circular Trailing edge. *International Journal of Heat and Fluid Flow*, Vol. 72, 20.

RAMAPRIYAN, B. R., PATEL, V. C. & SASTRY, M. S. 1982 The symmetric turbulent wake of a flat plate. *AIAA Journal*, Vol. 20 (9), 1228.

SATO, H. & KURIKI, K. 1961 The mechanism of transition in the wake of a thin flat plate placed parallel to a uniform flow. *Journal of Fluid Mechanics*, Vol. 11, 321.

THOMAS, F. O., & LIU, X. 2004 An experimental investigation of symmetric and asymmetric turbulent wake development in pressure gradient. *Physics of Fluids*, Vol. 16, (5), 1725.

TRITTON, J. D. 1959 Experiments on the flow past a circular cylinder at low Reynolds numbers. *Journal of Fluid Mechanics*, Vol. 6, 547.